ChemPubSoc Europe

DOI: 10.1002/slct.201600406

Chemistry SELECT Full Papers

Materials Science inc. Nanomaterials & Polymers

Co–templating Synthesis of Bimodal Mesoporous Silica for Potential Drug Carrier

Wei C. Chu,[a] Dong R. Peng,[a] Bishnu P. Bastakoti,[b] Malay Pramanik,[b] Victor Malgras,[b] Tansir Ahamad,[c] Saad M. Alshehri,[c] Yusuke Yamauchi,*[b, c] and Shiao W. Kuo*[a]

Bimodal mesoporous silica is prepared by co-templating method using PEO-*b*-PLA diblock copolymer and F127 triblock copolymer. The pore size distribution of the mesoporous silica is bimodal, based on small angle X-ray scattering, transmission electron microscopy, and nitrogen adsorption-desorption isotherms analyses, and can be divided into the larger pores, originating from PEO-*b*-PLA, and the smaller pores, originating from F127. In addition, we are able to ascertain that the F127 triblock copolymer not only produces the smaller pores, but also acts as a swelling agent in the formation of the larger pores. This novel bimodal mesoporous silica is further successfully employed as a drug-carrier for doxorubicin in ambient conditions.

Introduction

Ordered pores/channels arrangements, large pore diameters, high surface areas within small volume fractions, and high thermal stability are features that make mesoporous silica an ideal material for different applications such as sensing, separation, catalysis, filtering, optics, and electronics.[1-18] Usually, mesoporous silica is prepared with amphiphilic block copolymers as templates based on evaporation-induced self-assembly (EISA).[9-17] For example, the amphiphilic ABA-type poly(ethylene oxide-b-propylene oxide-b-ethylene oxide) triblock copolymer (PEO-*b*-PPO-*b*-PEO, Pluronic F127) has been used for the synthesis of mesoporous silica with a controlled mesostructured, from hexagonal cylinder to body-centered cubic (BCC), by changing the concentration of tetraethyl orthosilicate (TEOS).[10] In addition, diblock copolymers such as poly(ethylene oxide-*b*-caprolactone) (PEO-*b*-PCL),[11-12] poly(ethylene oxide-*b*-lactide) (PEO-*b*-PLA),[13] poly(ethylene oxide-*b*-L-lactide) (PEO-*b*-PLLA),[13] poly (ethylene oxide-*b*-methyl methacrylate) (PEO-*b*-PMMA)[14] and poly(ethylene oxide-*b*-styrene) (PEO-*b*-PS)[15–17] have been widely studied as templates to prepare mesoporous silica. However, these templates usually lead to unimodal pore distributions due to the presence of a single hydrophobic segment (PCL, PLA, PLLA, PMMA and PS). Similarly, while classical mesoporous materials, such as the SBA-15 and MCM-41, were widely reported for different applications, the unimodal pore size distribution leads to single adsorption characteristic.[5-8] Bimodal mesoporous materials are comparatively less studied. Recently, various bimodal mesoporous silica materials have been synthesized by co-templating. From the viewpoint of applications such as size-selective sorption, catalysis and drug release, bimodal mesoporous materials offer great advantages.[18-20]

We have previously reported that the poly(ethylene-*b*-ethylene oxide-*b*-ε-caprolactone) triblock copolymer can be successfully employed as a single template to prepare bimodal mesoporous silica.[21] The synthesis of triblock copolymers is difficult and time-consuming. In contrast, the co-template method, consisting in blending two different templates, is a relatively simpler approach. Zhao *et al.* synthesized bimodal mesoporous silica by using PEO-*b*-PMMA along with a cationic surfactant (alkyltrimethylammonium bromide, CTAB) as a co-template.[22] Sun *et al.* synthesized bimodal porous silica that enables independent control over small and large mesopore sizes by cross-linking mesoporous MCM-41 nanoparticles.[20] Reber *et al.* synthesized bimodal mesoporous silica through a partial pseudomorphic transformation of an ordered mesoporous starting material.[19] The co-template methods using F127 triblock copolymer and PEO-*b*-PCL diblock copolymer were also reported, providing dual-mesoporous silica with ultra-low refractive indices.[4]

In recent years, mesoporous silica was employed in a wide range of applications, including biology an drug delivery, due to their excellent stability and bio-compatibility.[23-30] Bimodal mesoporous silica possesses critical features for improving storage and drug delivery efficiencies. In this work, bimodal mesoporous silica is prepared by using a co-template method based on PEO-*b*-PLA diblock copolymer and F127 triblock copolymer at various mass ratios, combined with a TEOS matrix (Figure 1).

[a] *Dr. W. C. Chu, D. R. Peng, Prof. S. W. Kuo*
Materials and Optoelectronic Science Institution
National Sun Yat-Sen University
Center for Nanoscience and Nanotechnology
Kaohsiung, 804, Taiwan
E-mail: kuosw@faculty.nsysu.edu.tw

[b] *Dr. B. P. Bastakoti, Dr. M. Pramanik, Dr. V. Malgras, Prof. Y. Yamauchi*
World Premier International (WPI)
Research Center for Materials Nanoarchitectonics (MANA)
National Institute for Materials Science (NIMS)
1-1 Namiki, Tsukuba, Ibaraki 305–0044 (Japan)
E-mail: yamauchi.yusuke@nims.go.jp

[c] *Prof. T. Ahamad, Prof. S. M. Alshehri, Prof. Y. Yamauchi*
Department of Chemistry, College of Science
King Saud University
Riyadh 11451 (Saudi Arabia)

Supporting information for this article is available on the WWW under http://dx.doi.org/10.1002/slct.201600406

© 2016 Wiley-VCH Verlag GmbH & Co. KGaA, Weinheim

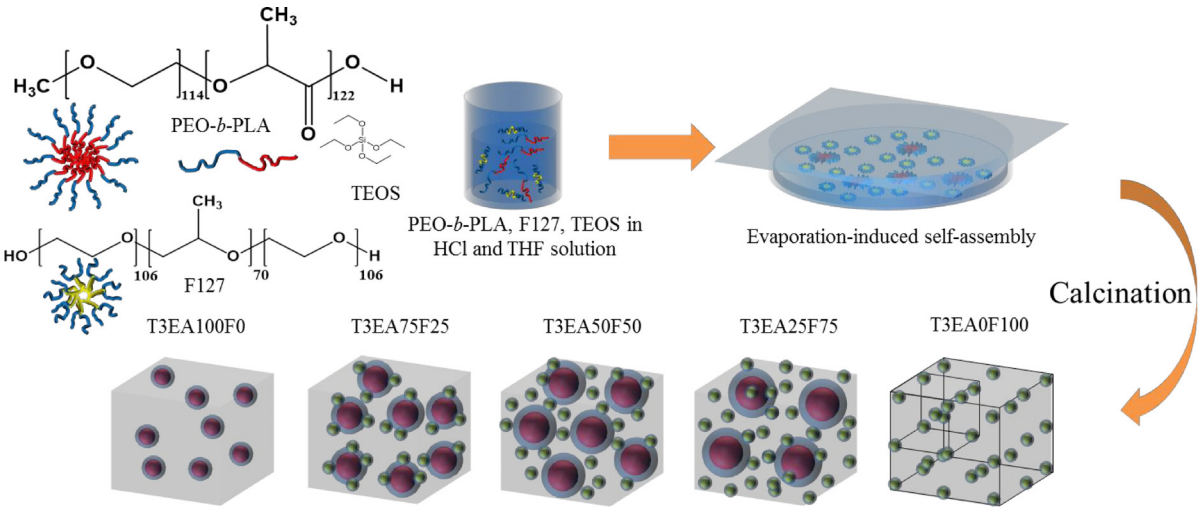

Figure 1. Scheme of mesoporous silica co-templated with PEO-*b*-PLA and F127 block copolymers.

Table 1. Textural properties of mesoporous silica templated by PEO-*b*-PLA/F127 co-templates.

Sample (TxEAyFz)[a]	*d* (nm)[b]	Pore size (nm)	S_{BET} (m^2g^{-1})[c]	Pore volume (cm^3g^{-1})
T1EA100F0	27.8	29.2	758	2.89
T1EA75F25	14.6, 36.9	11.7, 36.9	569	1.99
T1EA50F50	13.7	10.2, 32.8	521	1.24
T1EA25F75	13.3	5.8, 26.0	540	1.48
T1EA0F100	11.8	10.7	546	1.47
T3EA100F0	22.4	15.0	418	0.82
T3EA75F25	23.0	16.8	614	1.02
T3EA50F50	12.6, 33.1	5.7, 19.5	425	0.69
T3EA25F75	12.1, 48.3	6.7, 22.5	425	0.71
T3EA0F100	10.8	5.8	734	0.86
T5EA100F0	22.5	11.7	343	0.49
T5EA75F25	22.5	13.3	466	0.50
T5EA50F50	27.3	17.4	499	0.50
T5EA25F75	10.8, 36.9	4.0, 23.0	519	0.52
T5EA0F100	10.4	4.7	613	0.56
T10EA100F0	22.4	13.3	187	0.12
T10EA75F25	27.3	15.2	307	0.25
T10EA50F50	29.9	15.2	376	0.30
T10EA25F75	-	17.6	445	0.29
T10EA0F100	-	7.8	567	0.27

[a] *x* is the TEOS-to-total-template mass fraction; *y* and *z* are the templates mass percentage of PEO-*b*-PLA and F127, respectively.
[b] The *d*-spacing values were calculated from the first SAXS peak by the formula $d = 2\pi/q^*$.
[c] S_{BET} is the total BET surface area.

The co-templating method has several advantages over the single templating method regarding the synthesis of bimodal silica. The bimodal mesoporosity of the silica matrix is confirmed by small angle X-ray scattering (SAXS), transmission electron microscope (TEM), and nitrogen adsorption-desorption isotherms analyses. Finally, the bimodal mesoporous silica is loaded with doxorubicin and the effect of the bimodality on the kinetics of drug release is studied.

Results and Discussion

Characterization of bimodal mesoporous silicas co–templated by PEO-*b*-PLA/F127

Table 1 lists the samples synthesized in the current study (with different TEOS, PEO-*b*-PLA and F127 contents) and provides the structural information obtained from the adsorption-desorption isotherms analysis. The SAXS patterns and TEM images of the mesoporous silica based on a PEO-*b*-PLA template at different TEOS:PEO-*b*-PLA mass ratios (1:1, 3:1, 5:1 and 10:1) are shown in Figure S1. When the concentration of TEOS increases, the *d*-spacing of the mesoporous silica decreases along with the average pore size and the thickness of the wall increases. The nitrogen adsorption and desorption curves at different TEOS:PEO-*b*-PLA mass ratios (shown in Figure S2a) are type-IV isotherms. The BDDT classification has become the core of the modern IUPAC classification of adsorption isotherms.[31,32] The mesoporous silica at TEOS:PEO-*b*-PLA = 1:1 exhibits H_1-like hysteresis loops at values of P/P_0 ranging from 0.75 to 1.00, while the other ratios at TEOS:PEO-*b*-PLA = 3:1 and 5:1 lead to H_3-like hysteresis loops at values of P/P_0 ranging from 0.45 to 0.90, and at TEOS:PEO-*b*-PLA = 10:1 lead to H_3-like hysteresis loops at values of P/P_0 ranging from 0.35 to 0.90. The pore size distributions for the each mass ratio (1:1, 3:1, 5:1 and 10:1) were calculated from the isotherm data to be 29.2 nm,

© 2016 Wiley-VCH Verlag GmbH & Co. KGaA, Weinheim

15.8 nm, 11.7 nm and 13.3 nm, respectively, based on the Barrett-Joyner-Halenda (BJH) model (Figure S2b). From the TEM images in Figure S1b-e, the pore size distributions and *d*-spacings of the wormhole-like micelles are uniform, but the pore thickness increases with increasing the TEOS:PEO-*b*-PLA mass ratio.

Figure 2 shows the SAXS patterns of the bimodal mesoporous silica prepared in presence of TEOS and a PEO-*b*-PLA/F127 co-template with a TEOS:co-template mass ratio of = 3:1. The first scattering peak (q_1*) corresponding to the PEO-*b*-PLA template can be distinguished from the second peak (q_2*) which can be assigned to the F127 template, because of their different molecular weights. The SAXS of T1EA100F0 (Figure S3) showing hexagonal cylindrical characteristic peaks located at $1:3^{1/2}:7^{1/2}$, and corresponding to hexagonal cylindrical structure, supports TEM (top view and side view) observations of Figure S4a. In addition, the SAXS pattern of T3EA0F100 (Figure 2) exhibits sharp body centered cubic (BCC) characteristic peaks located at $1:2^{1/2}:3^{1/2}:4^{1/2}:5^{1/2}$, which can be assigned to a BCC structure, as confirmed by the TEM image in Figure 3e. As seen in Figure 2, when the F127:PEO-*b*-PLA mass ratio of the co-template increases, the q_1* *d*-spacing increases from 22.4 nm (for T3EA100F0) to 48.3 nm (for T3EA25F75), while the q_2* *d*-spacing is maintained at *ca.* 10 ~ 12 nm. The broadening of the q_2* peaks was observed, with the increase of the PEO-*b*-PLA, indicating that the long-range order of the BCC pattern become restricted to a much shorter range order, due to the presence of spherical structures, which is consistent with the TEM images in Figure 3b-3d. It can be concluded that parts of the F127 molecules are being inserted inside the PEO-*b*-PLA self-assembly through hydrogen bonding interaction within the ether groups of the PEO segments, ultimately leading to the swelling of the hydrophobic region and inducing the formation of bigger mesopores. Figure 4a shows the nitrogen adsorption-desorption curves related to the TEOS:co-templates = 3:1 mass ratio, which are also typical type-IV isotherms with H_2-type (ink-bottle) hysteresis loops, assigned to capillary condensation. The contribution in the relative pressure ranging from 0.45 to 0.95 is related to PEO-*b*-PLA and the one in the relative pressure range from 0.45 to 0.80 can be assigned to F127.[10,13] The adsorption isotherm curves of T3EA50F50 and T3EA25F75 have two distinguishable components. The pore size distribution curves exhibits two prominent peaks for T3EA50F50 and T3EA25F75 (Figure 4b). In Figure 3, the morphologies were controlled from the uniform micelles, to bimodal sphere, to BCC with the decreased PEO-*b*-PLA:F127 ratio. In the TEOS/co-templates = 3/1 mass ratio, the bimodal mesoporous silica are easily prepared by co-template method.

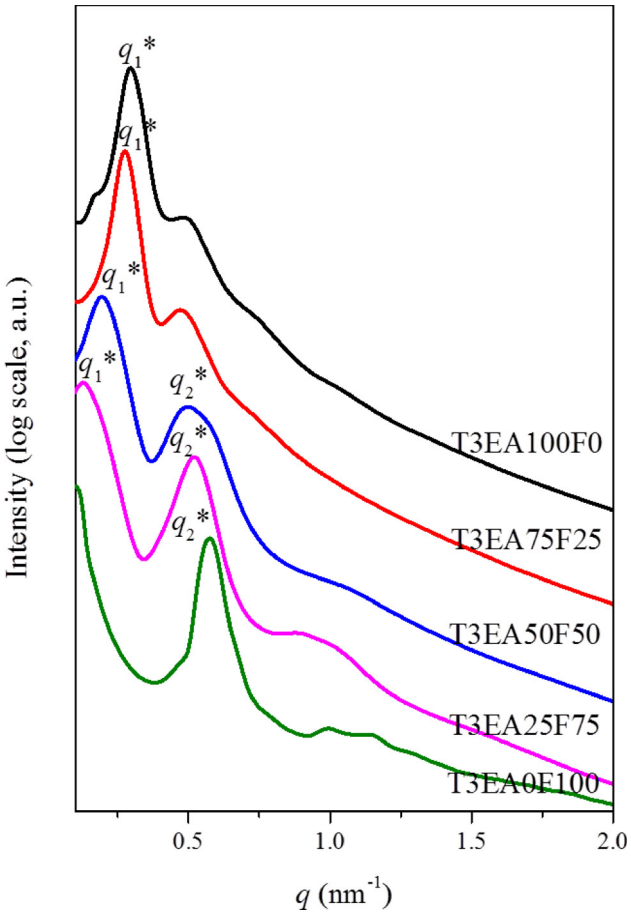

Figure 2. SAXS patterns of mesoporous silica prepared at TEOS:co-template ratio = 3:1 with various PEO-*b*-PLA:F127 mass ratios. The peaks indicated by q_1* correspond to the PEO-*b*-PLA-template and q_2* correspond to the F127 template.

The TEOS:co-templates mass ratio of 5:1 is investigated as well. On the SAXS spectra from Figure 5, the q_1* peaks can be assigned to the PEO-*b*-PLA template while the higher q_2* peaks correspond to the F127 template. Similarly, the q_1* *d*-spacing increases from 22.5 nm to 36.9 nm, while the q_2* *d*-spacing is mostly maintained at *ca.* 10 ~ 11 nm. The swelling of the pores originating from the presence of F127 in the co-template can clearly be observed on the TEM images (Figure 6b and 6c). With the concentration of F127 is increased, the q_1* *d*-spacing increases because part of F127 swell the hydrophobic region of PEO-*b*-PLA. In Figure 7, the nitrogen adsorption-desorption isotherm curves are also type-IV in nature with a H_2 hysteresis loop, and the mesoporous silica samples exhibit similar capillary condensation as for TEOS:co-templates = 3:1. Furthermore, T5EA25F75 also exhibits a two-step adsorption isotherm curves, two prominent peaks in the pore size distributions curve and both q_1* peak and q_2* peaks in the SAXS pattern (Figure 5), which is consistent with the TEM image in Figure 6d. With increasing the F127 content, the average pore size of the mesoporous silica increases (Figure 6). In addition, SAXS, TEM and nitrogen adsorption and desorption isotherms analyses were also carried on mesoporous silica samples with TEOS:co-templated mass ratios of 1:1 and 10:1 (see Table 1, and Figure S3-S8).

Bimodal (T3EA50F50) and unimodal (T3EA100F0 and T3EA0F100) mesoporous silica have been selected to be tested as drug carriers. In Figure 2, the SAXS pattern of T3EA50F50 shows two sharp peaks including the q_1* peak (q_1* = 0.2, *d*-spacing = 33.1 nm) and the q_2* peak (q_2* = 0.5, *d*-spacing = 12.6 nm). T3EA100F0 and T3EA0F100 exhibit sharp *q** peaks at

© 2016 Wiley-VCH Verlag GmbH & Co. KGaA, Weinheim

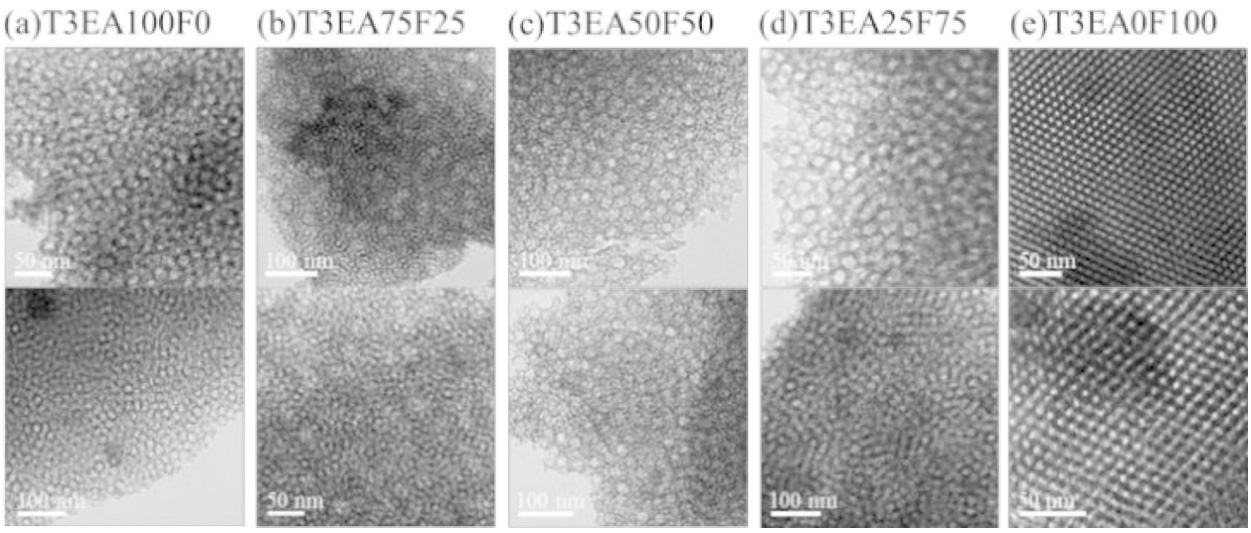

Figure 3. TEM images of mesoporous silica prepared at a TEOS:co-template ratio = 3:1 with various PEO-b-PLA:F127 mass ratios.

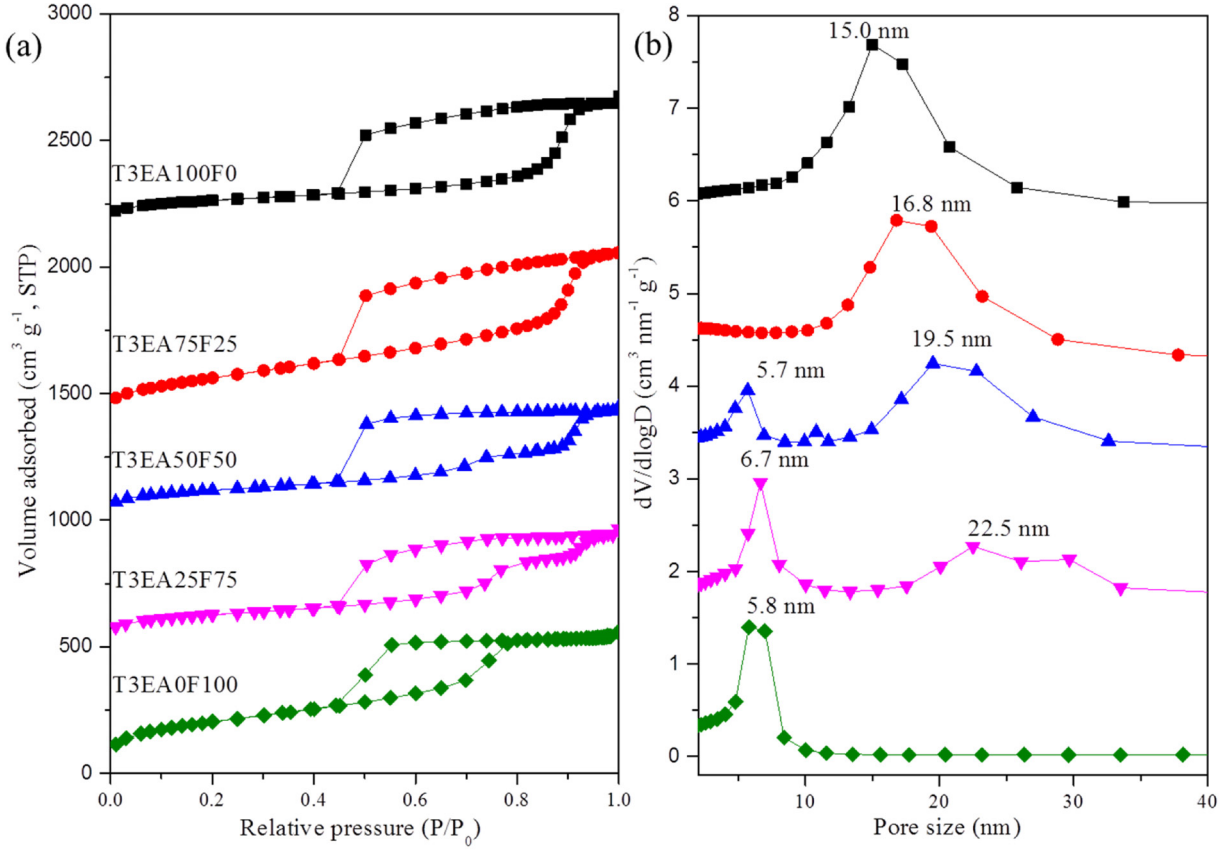

Figure 4. (a) Nitrogen adsorption-desorption isotherm and (b) pore size distribution curves of mesoporous silica prepared at a TEOS:co-template ratio = 3:1 with various PEO-b-PLA:127 mass ratios.

q^* = 0.28 and 0.58 (d-spacing = 22.4 nm and 10.8 nm), respectively. The isotherm curves (Figure 4a) also possess a H_2-type (ink-bottle) hysteresis loop generated by the overlapping capillary condensation steps assigned to PEO-*b*-PLA and F127. This specific feature is an indication of how hard it is for N_2 to adsorb and desorb, suggesting that the release time can be extended.[33] The pore size distribution curves of T3EA50F50 (Figure 4b) show two sharp peaks: one at 19.5 nm (from the PEO-*b*-

© 2016 Wiley-VCH Verlag GmbH & Co. KGaA, Weinheim

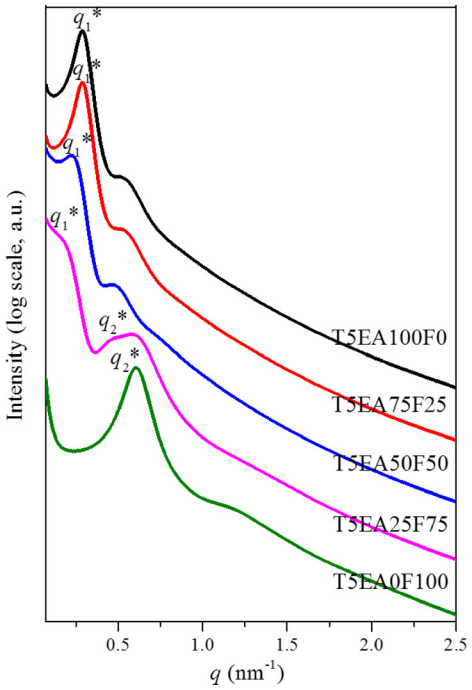

Figure 5. SAXS patterns of mesoporous silica prepared at a TEOS:co-template ratio = 5:1 with various PEO-*b*-PLA:F127 mass ratios. The peaks indicated by q1* are corresponding to PEO-*b*-PLA-template and q2* are corresponding to F127-template.

PLA template) and one at 5.7 nm (from the F127 template). Analogically, the pore size distributions of T3EA100F0 and T3EA0F100 are 15.0 nm and 5.8 nm, respectively. Previous studies have reported that the surface of mesoporous silica materilas can be functionalized through hydrogen bonding with doxorubicin molecules (DOX).[34] In Figure 8b, the time-dependent DOX-cumulative release exhibits a fast release of drug for each sample in the early stage. During the first 120 min, the DOX release percentage is of 10% for both T3EA50F50 and T3EA0F100, and only 6% for T3EA100F0. After 300 min, the release rate of T3EA100F0 and T3EA0F100 slows down, while T3EA50T50 maintains a similar release rate until 540 min. In other words, the bimodal mesoporous silica has a better release efficiency and cumulative release property than its unimodal counterparts. In order to determine the saturation, we extended the release time up to 1,800 min (shown up to 1,080 min in Figure 8). The DOX-cumulative releases at saturation for T3EA50F50, T3EA100F0 and T3EA0F100 are 31.0, 27.2 and 24.0%, and the DOX loading capacity are 72.2, 59.8 and 51.8 μg mg^{-1}, respectively. The drug release kinetics can be described by a power law: $(M_t/M_\infty) = kt^n$, where M_t is the concentration of drug released at a time t, M_∞ is the amount of drug released at saturation, k is a constant and n (with $0.5 \leq n \leq 1.0$) is the diffusion exponent related to the drug release mechanisms.[34-35] When $n = 1.0$, the release rate is independent of the time, thus it indicates swelling controlled mechanism for a zero order release.[33] When $n = 0.5$, the swelling diffusion kinetics follows a Fickian diffusion model. Between 0.5 and 1.0, the kinetics follows an anomalous transport (non-Fickian), so it effects by swelling and stresses.[33] In our case, the diffusion exponent (n) of T3EA100F0, T3EA50F50 and T3EA0F100 are 0.79, 0.61 and 0.69, respectively (In Table 2). Each sample thus fol-

Table 2. Textural properties of the drug delivery experiment

Sample	*k* (Constant)[a]	*n* (Diffusion exponent)[a]	Loading capacity[b] (μg mg^{1})
T3EA100F0	0.13	0.79	51.8
T3EA50F50	0.52	0.61	72.2
T3EA0F100	0.31	0.69	59.8

[a] *n* and *k* values were calculated from the simple linear regression for the power law equation.
[b] Loading capacities are calculated from the calibration curve within 30 h.

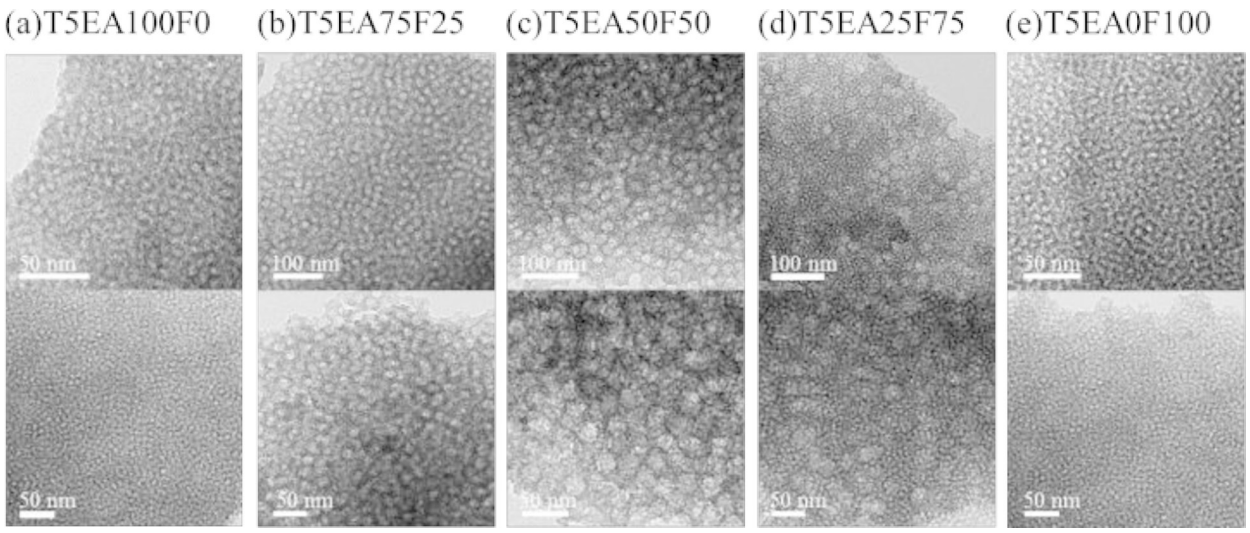

Figure 6. TEM images of mesoporous silica prepared at a TEOS:co-template ratio = 5:1 with various PEO-b-PLA:F127 ratios.

© 2016 Wiley-VCH Verlag GmbH & Co. KGaA, Weinheim

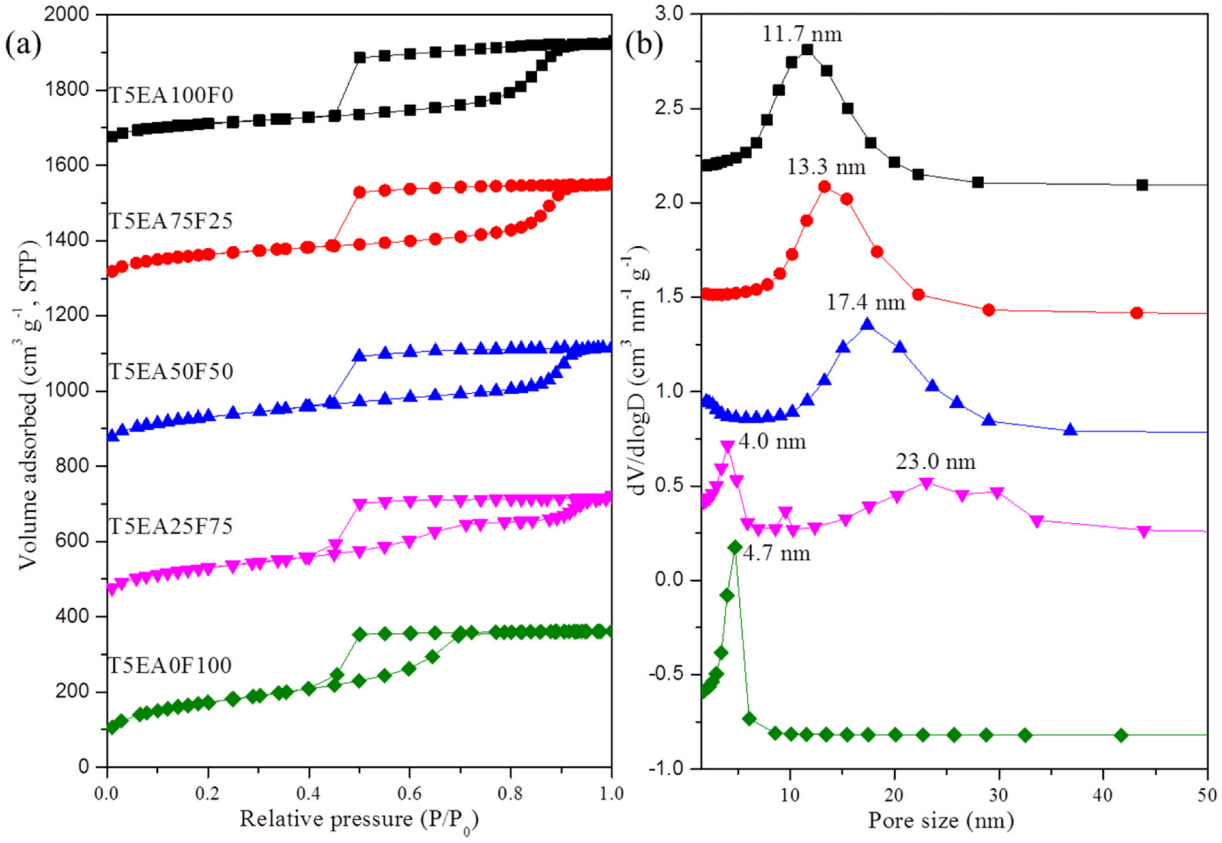

Figure 7. (a) Nitrogen adsorption-desorption isotherm and (b) pore size distribution curves of mesoporous silica prepared at a TEOS:co-template ratio = 5:1 with various PEO-b-PLA:F127 mass ratios.

lows non-Fickian transport, which has been often reported as a typical release property of porous materials.[34-35] The bimodal mesoporous silica have better loading capacity and cumulative release efficiency than single-model mesoporous silica.

Conclusions

Bimodal mesoporous silica is prepared by co-templating method using PEO-*b*-PLA diblock copolymer and F127 triblock copolymer with various mass ratios. According to the SAXS, TEM and nitrogen adsorption-desorption isotherms analysis, the large pores are formed by the PEO-*b*-PLA template while the small pores are formed by F127 template. In addition, the F127 not only produced the small size pores but also acts as a swelling agent to form larger pore. Using this method, it is possible to easily prepare bimodal mesoporous materials with fine-tuning over the pore diameter. Unimodal and bimodal mesoporous silica are used for DOX adsorption and release. It is found that bimodal mesoporous silica shows higher loading capacity and better cumulative release. The fine-tuning of the average pore size and size distribution in bimodal silica can enable the incorporation of size-controlled loading and delivery of multiple drugs in future biomedical applications.

Supporting Information

Supporting information contains detailed description including the materials of experimental; materials synthesized steps, total experimental steps, characterization, and the detailed other experimental data of bimodal mesoporous silica templated by different molecular weight of PEO-*b*-PLA and F127.

Acknowledgements

This study was financially supported by the Ministry of Science and Technology, Taiwan, under contracts MOST 103–2221-E-110-079-MY3. W.C.C. would like to thank 2014 New Partnership Program for the Connection to the Top Labs in the World, also supported by the Ministry of Science and Technology, Taiwan, under contracts MOST 103–2911-I-110-513 that helped initiate this study. S.M.A. and Y.Y. extend their appreciation to the Visiting Professor Program (VPP) supported by the Deanship of Scientific Research, King Saud University.

Keywords: Bimodal mesoporous silica · Self-assembly · Doxorubicin · Drug Carriers · Mesoporous materials

[1] V. Malgras, Q. Ji, Y. Kamachi, T. Mori, F. K. Shieh, K. C. W. Wu, K. Ariga, Y. Yamauchi, *Bull. Chem. Soc. Jpn.* **2015**, *88*, 1171-1200.

© 2016 Wiley-VCH Verlag GmbH & Co. KGaA, Weinheim

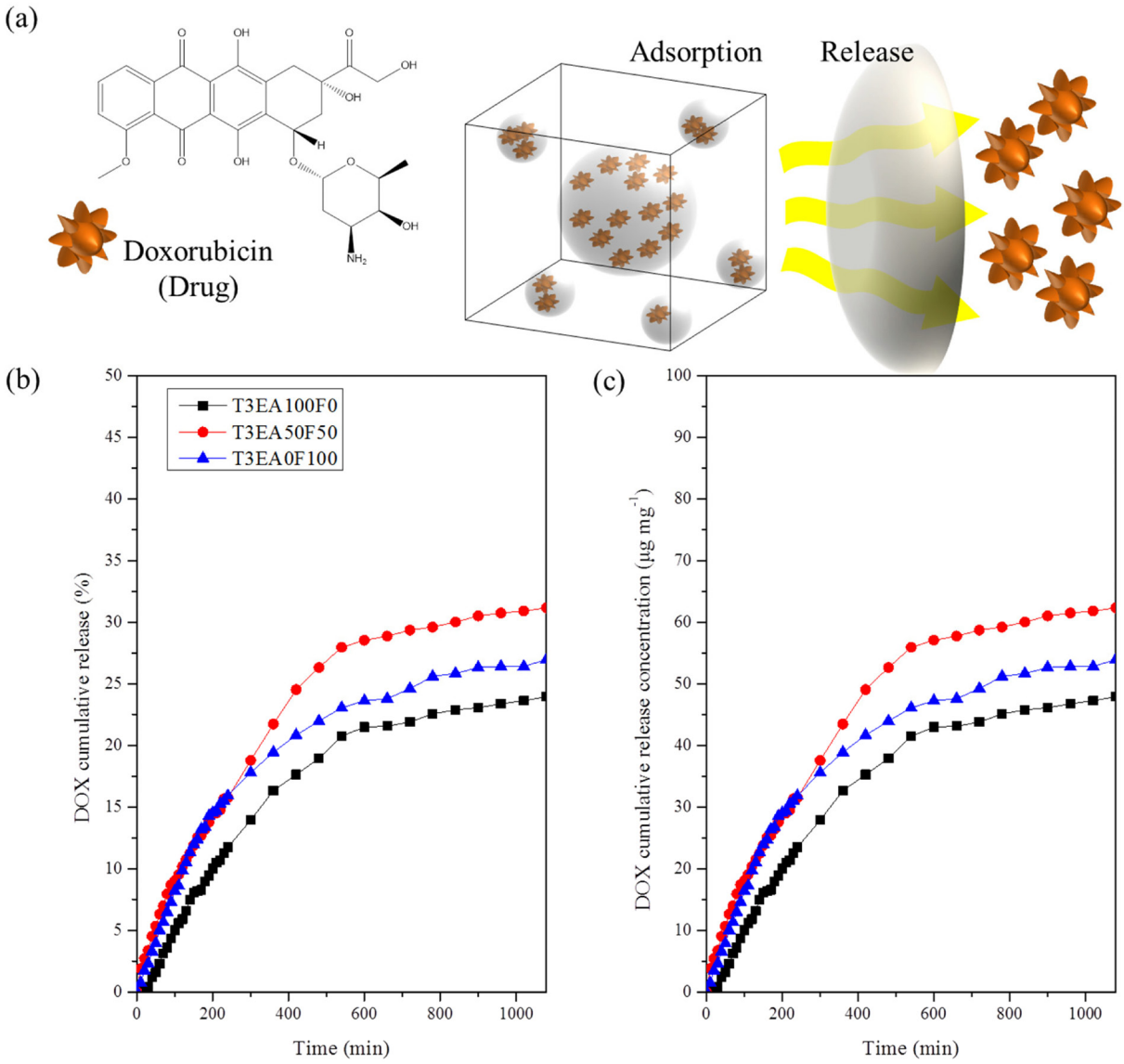

Figure 8. (a) The scheme of DOX-release (b) DOX cumulative release (c) DOX cumulative release concentration.

[2] Y. S. Lu, B. P. Bastakoti, M. Pramanik, V. Malgras, Y. Yamauchi, S.W. Kuo, *Chem. Eur. J.* **2016**, *22*, 1159–1164.
[3] K. Ariga, A. Vinu, Y. Yamauchi, Q. Ji, J. P. Hill, *Bull. Chem. Soc. Jpn.* **2012**, *85*, 1–32.
[4] C. C. Liu, J. G. Li, S. W. Kuo, *RSC Adv.* **2014**, *4*, 20262–20272.
[5] P. Yang, D. Zhao, D. I. Margolese, B. F. Chmelka. G. D. Stucky, *Chem. Mater.* **1999**, *11*, 2813–2826.
[6] B. P. Bastakoti, S. H. Liao, M. Inoue, S. Yusa, M. Imura, K. Nakashima, K. C. W. Wu, Y. Yamauchi, *Sci. Technol. Adv. Mat.* **2013**, *14*, 044402.
[7] S. Giret, M. W. C. Man, C. Carcel, *Chem. Eur. J.* **2015**, *28*, 13850–13865.
[8] B. P. Bastakoti, K. C. W. Wu, M. Inoue, S. Yusa, K. Nakashima, Y. Yamauchi, *Chem. Eur. J.* **2013**, *19*, 4812–4817..
[9] J. G. Li, S. W. Kuo, *RSC Adv.* **2011**, *1*, 1822–1833.
[10] W. C. Chu, S. F. Chiang, J. G. Li, S. W. Kuo, *RSC Adv.* **2014**, *4*, 784–793.
[11] J. G. Li, Y. H. Chang, Y. S. Lin, S. W. Kuo, *RSC Adv.* **2012**, *2*, 12973–12982.
[12] W. C. Chu, C. X. Lin, S. W. Kuo, *RSC Adv.* **2014**, *4*, 61012–61021.
[13] O. Altukhov, S. W. Kuo, *RSC Adv.* **2015**, *5*, 22625–22637.
[14] Y. Deng, C. Liu, D. Gu, T. Yu, B. Tu, D. Zhao, *J. Mater.Chem.* **2008**, *18*, 91–97.
[15] Y. Deng, J. Liu, C. Liu, D. Gu, Z. Sun, J. Wei, J. Zhang, L. Zhang, B. Tu, D. Zhao, *Chem. Mater.* **2008**, *20*, 7281–7286.
[16] Y. Deng, T. Yu, Y. Wan, Y. Shi, Y. Meng, D. Gu, L. Zhang, Y. Huang, C. Liu, X. Wu, D. Zhao, *J. Am. Chem. Soc.* **2007**, *129*, 1690–1697.
[17] E. Bloch, P. L. Llwewllyn, T. Phan, D. Bertin, V. Hornebecq, *Chem. Mater.* **2009**, *21*, 48–55.
[18] F. Zhang, Y. Yan, Y. Meng, Y. Xia, B. Tu, D. Zhao, *Microporous Mesoporous Mater.* **2007**, *98*, 6–15.
[19] M. J. Reber, D. Brühwiler, *Dalton Trans.* **2015**, *44*, 17960–17967.
[20] J. H. Sun, Z. Shan, T. Maschmeyer, M. O. Coppens, *Langmuir* **2003**, *19*, 8395–8402.
[21] J. G. Li, R. B. Lin, S. W. Kuo, *Macromol. Rapid Commun.* **2012**, *33*, 678–682.
[22] J. Wei, Q. Yue, Z. Sun, Y Deng, D. Zhao, *Angew. Chem. Int. Ed.* **2012**, *51*, 6149–6153.
[23] A. M. Chen, M. Zhang, D. Wei, D. Stueber, O. Taratula, T. Minko, H. He, *Small* **2009**, *5*, 2673–2677.
[24] I. I. Slowing, B. G. Trewyn, V. S. Y. Lin, *J. Am. Chem. Soc.* **2007**, *129*, 8845–8849.

© 2016 Wiley-VCH Verlag GmbH & Co. KGaA, Weinheim

[25] M. Vallet-Regi, A. Ramila, R. P. del Real, J. Perez-Pariente, *Chem. Mater.* **2001**, *13*, 308–311.
[26] N. K. Mal, M. Fujiwara, Y. Tanaka, *Nature* **2003**, *421*, 350–353.
[27] M. Vallet-Regi, F. Balas, D. Arcos, *Angew. Chem. Int. Ed.* **2007**, *46*, 7548–7558.
[28] I. I. Slowing, B. G. Trewyn, S. Giri, V. S. Y. Lin, *Adv. Funct. Mater.* **2007**, *17*, 1225–1236.
[29] Q. Zhan, J. Qian, X. Li, S. He, *Nanotechnology* **2010**, *21*, 055704.
[30] X. Jiang, T. L. Ward, Y. S. Cheng, J. Liu, C. J. Brinker, *Chem. Commun.* **2010**, *46*, 3019–3021.
[31] D. R. Radu, C. Y. Lai, J. W. Wiench, M. Pruski, V. S. Y. Lin, *J. Am. Chem. Soc.* **2014**, *126*, 1640–1641.
[32] J. Rouquerol, D. Avnir, C. W. Fairbridge, D. H. Everett, J. M. Haynes, N. Pernicone, J. D. F. Ramsay, K. S. W. Sing, K. K. T. Unger, *Pure Appl. Chem.* **1994**, *66*, 1739–1758.
[33] J. Siepmann, N. A. Peppas, *Adv. Drug Deliver. Rev.* **2001**, *48*, 139-157.
[34] H. Y. Lian, Y. H. Liang, Y. Yamauchi, K. C.W. Wu, *J. Phys. Chem. C* **2011**, *115*, 6581–6590.
[35] P. L. Ritger, N. A. Peppas, *J. Control Release* **1987**, *5*, 23–36.

Submitted: April 18, 2016
Accepted: April 26, 2016

© 2016 Wiley-VCH Verlag GmbH & Co. KGaA, Weinheim